

Deep Learning Classification of Cheatgrass Invasion using Biophysical and Remote Sensing Data

Kyle Larson^{*}¹ and Aaron Tuor[†]¹

¹Pacific Northwest National Laboratory

September 12, 2017

Contents

1	Introduction	2
2	Related Work	3
2.1	Cheatgrass Mapping	3
2.2	Machine Learning Methods for Geo-spatial Prediction	3
2.3	PNNL study	3
2.4	Other works	3
3	Data Set	4
3.1	Field Measurements	4
3.2	Bio-physical Data	4
3.2.1	Potential relative radiation	4
3.2.2	DAYMET	5
3.2.3	Growing degree days	5
3.2.4	PRISM	5
3.3	Ecological Data	5
3.3.1	Ecoregions	6
3.3.2	LANDFIRE Landcover	6
3.4	Satellite Imagery	6
3.4.1	Normalized Difference Vegetation Index	7
3.4.2	Enhanced Vegetation Index (EVI)	7
3.4.3	MODIS (annual, seasonal)	7
3.4.4	Landsat (annual, seasonal)	7
3.5	Data Synopsis	7
4	Methods	8
4.1	Baseline Models	8
4.2	Deep Learning Models	8
4.2.1	Deep Neural Network	8
4.2.2	Recurrent Neural Network	8
4.3	Performance on Field measurement locations	11
4.4	Experimental Setup	11

^{*}kyle.larson@pnnl.gov

[†]aaron.tuor@pnnl.gov

5 Results and Analysis	11
5.1 Performance on Field measurement locations	11
5.1.1 Quantitative assessment	11
5.1.2 Training Statistics	11
5.1.3 Qualitative assesment	11
5.2 Performance on Full Study Region	13
5.2.1 Pixel-wise count of cheatgrass class across model predictions	13
5.2.2 Block statistics (count) of cheatgrass class (analogous to block area), then look at range of block counts	13
6 Conclusion and Future Work	13

Abstract

In this study we explore deep learning approaches which incorporate geophysical data and readings from multiple remote sensing platforms for predictive mapping of vegetation over very large, ecologically diverse regions. We focus specifically on mapping an invasive exotic annual grass, cheatgrass (*Bromus tectorum*), that has become a major land management issue in the Western United States. We explore the relative advantages of deep neural networks to integrate imagery from the LandSat7 and MODIS platforms which have complementary advantages in their spectral bandwidth, spatial resolution, and temporal frequency. We show that integrating imagery from multiple platforms is beneficial to the predictive mapping of cheatgrass in the Western United State's historic range of Sage Grouse. Our analysis of prospective machine learning models demonstrates that a deep neural network can more effectively take advantage of the signal from multiple platforms than traditional classification models such as Random Forest, and Linear Discriminant Analysis for the classification of cheatgrass.

1 Introduction

Accurate and up to date maps of vegetation coverage are critical assets for land management agencies tasked with mitigating damage wrought by invasive species. A variety of methods have been developed to map invasive annual grasses from satellite and aerial imagery, each uniquely tailored to the limitations of the imagery. Current practices usually involve choosing one platform best suited for the study, although more than one may potentially be useful, e.g., using finer spatial resolution imagery may improve results, but doing so comes with concomitant loss of temporal resolution which is also important for detecting species like invasive cheatgrass which has maintained a growth cycle distinct from native vegetation.

Introduced in the late 19th-century, cheatgrass is now found in every state in the contiguous U.S.. Nowhere has its invasion been more prevalent than in western states where it has become a dominant component in many shrubland and grassland ecosystems. It is now estimated to dominate at least 40,000 km² in the states of Nevada and Utah alone. Cheatgrass invasion poses a variety of threats to ecosystem function, rangeland health, and human safety. A central thread to many of these threats is the increase in fine fuels associated with cheatgrass, which can lead to increased fire frequency and irreversible loss of native vegetation and wildlife habitat. Following a fire, cheatgrass is able to more effectively compete with native vegetation, giving rise to a positive feedback cycle of further invasion and fire. [Refs: Mack 1981; Pellatt 1996; Bradley & Mustard 2005; USDA Plant Database]

While cheatgrass is considered ubiquitous throughout much of the western U.S., detailed spatial information about its presence and abundance are still lacking for much of its range within this region. Previous efforts to map cheatgrass have focused on core areas of invasion such as the Great Basin and Snake River Plain. These efforts help paint a clearer picture of cheatgrass invasion in the western U.S., but their disparate nature (due to differing extents, methods, data, and focal periods) prevents easily reconciling them to inform range-wide management decisions. Conversely, mapping cheatgrass (or other vegetation) at a range-wide scale is also not straightforward or without its challenges; most notably the need for a greater volume of training and input predictor data to adequately model the phenomenon across many ecological gradients. [Refs:]

The study area encompasses a large part of the Intermountain West as well as portions of Montana, Wyoming, Colorado, and New Mexico east of the Rockies. The areal extent of the area identified as the historic sage-grouse range covers more than 308 million acres and includes portions of southern Alberta and British Columbia, Canada. This study focused on the U.S. portion of the sage-grouse range, which is approximately 288 million acres. Figure 1 shows the region considered and location of field samples.

2 Related Work

2.1 Cheatgrass Mapping

A variety of methods to map cheatgrass are described in the literature, ranging from imagery-driven methods that focus on spectral signatures or phenological indicators of cheatgrass to ecological niche modeling approaches aimed at mapping biophysical and climatic predictors. Much attention has been given to deriving phenological indicators of cheatgrass presence from overhead imagery (typically using spectral indices such as the Normalized Difference Vegetation Index, or NDVI) because its life cycle differs from many of the native plant species in its western range. Cheatgrass is a winter annual that may begin growth in the late fall and senesce in late spring, whereas many native plants begin growing in mid to late spring and continue growth through summer under favorable precipitation conditions. Thus, cheatgrass presence can be identified indirectly by comparing pixel-chronologies of NDVI, particularly in years when winter or early spring precipitation is [Refs: Rice et al. 1992; Loik 2007; Bradley 2009;] Phenological - attempt to exploit seasonal differences in growth of target and non-target species Can be highly variable across years, plant communities, and regions

Often target specific time periods to optimize detection of phenological signatures

- Spectral
- Biophysical
- Studies that attempt to combine these approaches?

2.2 Machine Learning Methods for Geo-spatial Prediction

Machine learning methods have become increasingly popular for remote sensing classification due to their ability to model complex class signatures, accept a variety of input data, and often outperform traditionally used parametric methods. Some of more commonly used machine learning methods in remote sensing include support vector machines (SVMs), Random Forests (RFs), single decision trees (DTs), boosted DTs, k-nearest neighbor (k-NN), and artificial neural networks (ANNs). While there has been considerable use and comparison of these as well as other machine learning methods not mentioned, there appears to be little consensus on whether one is more superior than the others. A number of excellent reviews of these machine learning methods in remote sensing exist, which we defer to for readers seeking more in-depth information and guidance on those specific methods. Here, we focus on illustrating the use and performance of a newer and rapidly growing class of machine learning methods called deep learning for classification in remote sensing, with an emphasis on providing an applied perspective from multiple domains. [Refs: Maxwell et al. 2018; Maxwell et al. 2015; Crisci et al. 2012; Lu & Weng 2007; Mountrakis et al. 2011; Rodriguez-Galiano et al. 2012; Rogan et al. 2008; Shao et al. 2012]

2.3 PNNL study

Impetus for previous study

In 2016, PNNL developed a statistical model to map the occurrence of cheatgrass in the Intermountain West that uses satellite-based Normalized Difference Vegetation Index (NDVI) a widely used spectral index for mapping cheatgrass, vegetation, and other phenomena and biophysical parameters. NDVI was derived from NASA's Moderate Resolution Imaging Spectroradiometer (MODIS) which offers low- spatial, high-temporal resolution imagery that is well-suited for assessing land cover over large geographic areas. The model achieved an acceptable level of accuracy for the study area (71%), but accuracy was variable when examined at finer scales.

2.4 Other works

- Land cover classification based on NDVI using LANDSAT8 time series: A case study Tirupati region [6]
- Hyperspectral remote sensing of vegetation [9]
- Multispectral and hyperspectral remote sensing for identification and mapping of wetland vegetation: a review [1]
- A review of hyperspectral remote sensing and its application in vegetation and water resource studies [4]
- Identification of invasive vegetation using hyperspectral remote sensing in the California Delta ecosystem [5]

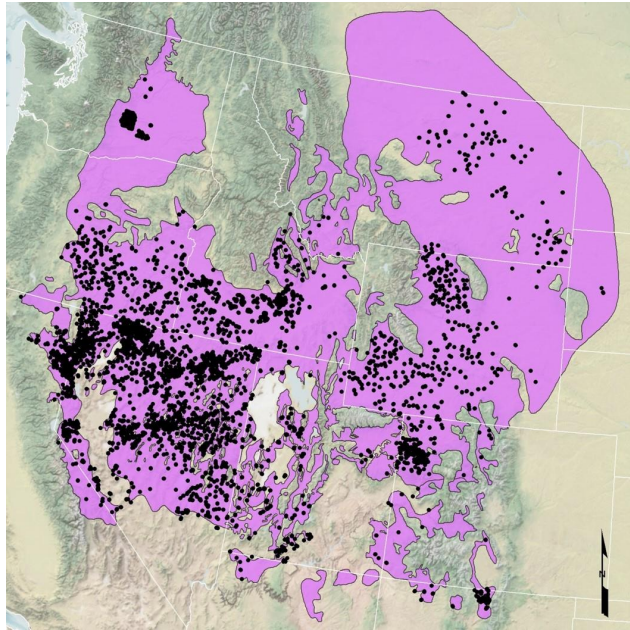


Figure 1: Study Region

- Mapping salt-marsh vegetation by multispectral and hyperspectral remote sensing [2]

3 Data Set

Within the study area boundaries, we solicited more than 24,000 field measurements from various sources to gather information on cheatgrass occurrence. Accompanying these field measurements are bio-physical measurements (weather and soil data), and ecological data, as well as satellite imagery gathered from the MODIS and LandSat platforms.

3.1 Field Measurements

Figure 2 provides the field measurement datasets and sources considered, although not all data sources and data were accepted for use. Data were reviewed for completeness, geographic accuracy, and quality of data source. Review of the field measurement dataset allowed us to identify 6,650 measurement points that could potentially be used for modeling. All field data were collected along transects ranging from 25m to 100m in length. Point intercept data and plot frame (0.25 m to 1 m) data taken along the transects were summarized to calculate percent canopy cover of *Bromus tectorum* and *B. rubens*. The introduced, annual grass, red brome (*B. rubens*) was included because it poses a very similar threat in terms of modifying fire regimes, and its life history characteristics are similar to cheatgrass.

3.2 Bio-physical Data

Bio-physical datasets used for model development included the elevation, potential relative radiation index (PRR) (Pierce et al. 2005), and a growing degree day index. Spatially interpolated climate data (precipitation, temperature) for the study area was acquired from the PRISM (Parameter-elevation Regressions on Independent Slopes Model) Climate Group (Daly et al. 1994; Daly et al. 2008; DiLuzio et al. 2008) and the Daily Surface Weather and Climatological Summaries (DAYMET) program (Thornton et al. 1997; Thornton et al. 2014).

3.2.1 Potential relative radiation

The PRR is a unitless index of available solar radiation for photosynthetic activity at a given location that takes into account the influence of geographic position, seasonal and daily variation in solar inclination, and topography. PRR was calculated by summing digital hillshade interpolations for a given period of interest as described by Pierce et al. (2005). Hourly hillshade interpolations were performed for daylight hours of one day of the month that most closely represents the average solar period for the month (i.e., $PRR = \text{Sum} [\text{Hillshade}_{i-j}, m-n], \text{hours } i-j \text{ for each representative}$

Table 2.1. Data Source and Number of Field Measurements Evaluated.

Description	Number of Field Measurements Reviewed	Number of Field Measurements Accepted
BLM Assessment, Inventory, and Monitoring Program	2043	1927
BLM Landscape Monitoring Framework	2335	2222
Global Invasive Species Information Network	4292	0
Joint Base Lewis-McCord Yakima Training Center	382	375
PNNL – Birds of Prey field campaign	92	81
PNNL – Hanford Vegetation	39	39
PNNL – Owyhee field campaign	30	29
PNNL – Shoshone field campaign	95	89
USGS SAGEMAP GIS database	820	818
Sagebrush Steppe Treatment Evaluation Project	1086	1070
U.S. Forest Service Forest Inventory Analysis	13170	0
Total	24384	6650

Figure 2: Field Data

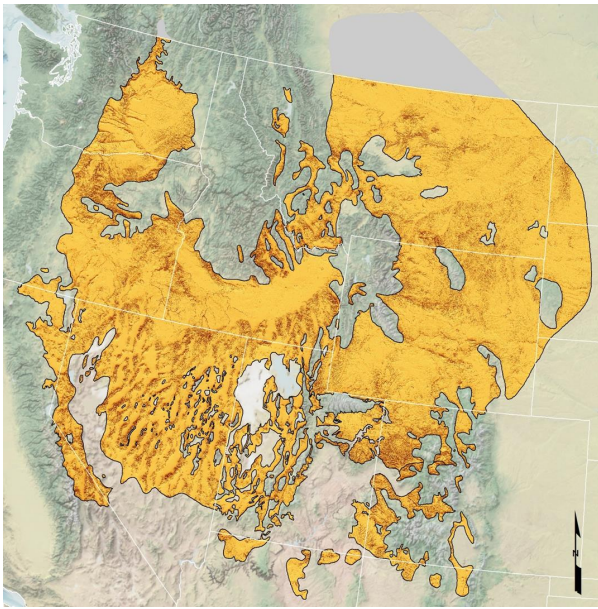


Figure 3: Potential Relative Radiation Index (light orange to dark orange illustrates high to low PRR).

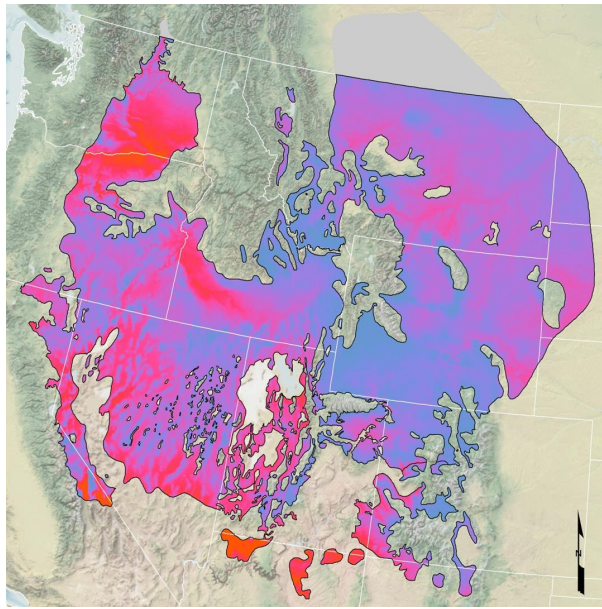


Figure 4: Cumulative Growing Degree Day (blue to red illustrates low to high GDD).

day of months m-n). PRR calculated for use in this study reflects the solar conditions between October and June, which encompasses the bulk of the growing season of cheatgrass across the study area.

3.2.2 DAYMET

DAYMET provides gridded estimates of daily weather parameters for North America at a 1-km resolution, including daily continuous surfaces of minimum and maximum temperature and precipitation. DAYMET daily minimum and maximum temperature data were acquired to calculate growing degree day index for the study area.

3.2.3 Growing degree days

Using the DAYMET daily minimum and maximum temperature data from 1 October 2014 to 30 April 2015, the cumulative growing degree day (GDD) index was calculated to represent the relative period of time when temperatures are suitable for plant growth (Figure 2.3).

The cumulative GDD between October 1 and April 30 was calculated on a daily basis: $[(T_{max} - T_{min})/2] \cdot w$ where w is the minimum temperature for growth of cheatgrass (assumed to be 0C or 32F), and summed for the period. Negative values were set to 0.

3.2.4 PRISM

PRISM uses point measurements of climate data and a digital elevation model of terrain to estimate continuous gridded surfaces of monthly climate elements at a 4-km resolution. PRISM 30-year mean monthly and 30-year mean annual precipitation, minimum temperature, and maximum temperature (totaling 39 separate climate variables) were obtained to explore relationships between cheatgrass occurrence and general climate patterns. We also derived several seasonal cumulative precipitation and average minimum and maximum temperature variables from PRISM data that correspond to important seasonal periods during the life history of cheatgrass.

3.3 Ecological Data

Our data set includes high level ecological data in the form ecoregions, and land cover classification.

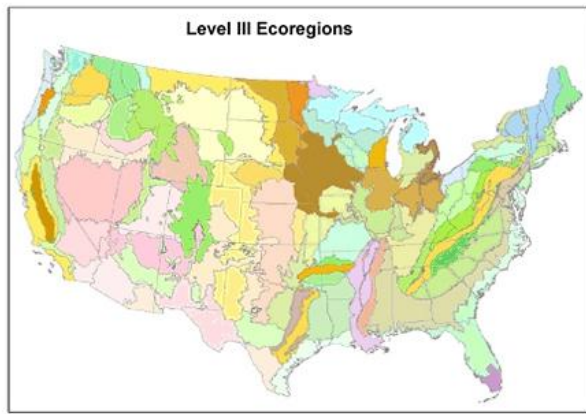


Figure 5: Figure from <https://www.epa.gov/eco-research/ecoregions>

Region Number	%	Region Name
4	0	Cascades
5	0	Sierra Nevada
9	1.9	Eastern Cascades slopes and foothills
10	8.7	Columbia plateau
11	1.7	Blue Mountains
12	9.3	Snake River plain
13	36	Central basin and range
15	0	Northern Rockies
14	0	Mojave basin and range
16	0.2	Idaho batholith
17	1.2	Middle Rockies
18	7.6	Wyoming basin
19	0.3	Wasatch and Uinta Mountains
20	3.7	Colorado plateaus
21	0.02	Southern Rockies
22	1.2	Arizona, New Mexico plateaus
23	0	Arizona, New Mexico Mountains
25	0.02	Wester high plains
41	0	Canadian Rockies
42	0.05	Northwestern glaciated plains
43	2	Northwestern great plains
77	0	North Cascades
80	25.3	Northern basin and range

Table 1: Study area ecoregions

3.3.1 Ecoregions

Ecoregions are areas which contain similar collections of plant and animal life, and similar ecological conditions such as geology, landforms, soils, vegetation, climate, land use, and water resources [7, 8, 3]. The study area spans 23 of the 182 level III ecoregions as defined by the U.S. Environmental Protection Agency (EPA) and the Commission for Environmental Cooperation (CEC). The ecoregion classifications for the study area were retrieved from the EPA hosted GIS data sets¹. Figure 5 shows the distributions of 16 ecoregions contained among the field measurement locations, while Table 1 shows the distribution of ecoregions throughout the study area.

3.3.2 LANDFIRE Landcover

Categorical value for vegetation cover type generalized from LANDFIRE (www.landfire.gov) vegetation data. 15 classes.

3.4 Satellite Imagery

For each location i in the full study region, we have retrieved yearly and seasonal image data from the MODIS and LandSat platform and derived vegetation indexes.

¹<https://www.epa.gov/eco-research/ecoregions>

Column	Band/Index
$M_{:,1}$	NDVI
$M_{:,2}$	EVI
$M_{:,3}$	Blue (B)
$M_{:,4}$	Red (R)
$M_{:,5}$	Near Infra-Red (NIR)
$M_{:,6}$	Mid Infra-Red (MIR)
$M_{:,7}$	dNDVI
$L_{:,1}$	dNDVI
$L_{:,2}$	Blue (B)
$L_{:,3}$	Green (G)
$L_{:,4}$	Red (R)
$L_{:,5}$	Near Infra-Red (NIR)
$L_{:,6}$	Short Wave Infra-Red 1 (SWIR1)
$L_{:,7}$	Thermal, low gain channel (T1)
$L_{:,8}$	Thermal, high gain channel (T2)
$L_{:,9}$	Short Wave Infra-Red 2 (SWIR2)

Table 2: Columns for MODIS spectral bands and vegetation indexes.

Table 3: Columns for LandSat spectral bands and vegetation indexes.

3.4.1 Normalized Difference Vegetation Index

NDVI values provided by the LandSat [10] and MODIS platforms are calculated as a ratio between the red (R) and near infrared (NIR) values as:

$$NDVI = (NIR - R)/(NIR + R) \quad (1)$$

We define dNDVI as the peak NDVI (over a span of a year or a season) minus long-term median annual peak NDVI (across the years we have images for).

3.4.2 Enhanced Vegetation Index (EVI)

EVI incorporates an L value to adjust for canopy background, C values as coefficients for atmospheric resistance, and values from the blue band (B) in order to reduce the background noise, atmospheric noise, and saturation [10].

$$EVI = G * ((NIR - R)/(NIR + C_1 * R - C_2 * B + L)) \quad (2)$$

3.4.3 MODIS (annual, seasonal)

The MODIS annual and seasonal composite imagery data consists of 250m resolution pixel values associated with each study region location i . We have composite annual, spring, and summer pixel values for each location in the study area for each year from 2001-2016. MODIS composite pixels are formed as the band or index value at the time of the peak NDVI value during the respective time range (spring, summer, or entire year). Introducing some notation we define three matrices $M_{\text{annual}}^{(i)}$, $M_{\text{spring}}^{(i)}$, and $M_{\text{summer}}^{(i)}$ for each study location i . Table 2 shows the spectral bands and derived indices that form a each matrix $M \in \mathbb{R}^{16 \times 7}$ of values with rows corresponding to the year, and columns corresponding to the spectral band or derived index.

3.4.4 Landsat (annual, seasonal)

The LandSat imagery differs from the MODIS imagery in resolution, spectral bands, years of operation, and composite product preparation. It consists of 30m resolution pixel values from the years 2003-2012. As in the case of MODIS, for convenience we define three matrices $L_{\text{annual}}^{(i)}$, $L_{\text{spring}}^{(i)}$, and $L_{\text{summer}}^{(i)}$ for each study location i . Table 3 shows the spectral bands and derived indices that form a each matrix $L \in \mathbb{R}^{10 \times 9}$ of values with rows corresponding to the year, and columns corresponding to the spectral band or derived index.

3.5 Data Synopsis

Tables 4, 5, and 6 contain brief descriptions of all variables used in modeling cheatgrass coverage. The complete set of data used in training predictive mapping models consists of 6602 locations with available field measurements due to missing values from 49 data points in the original data set. We define, $w \in \mathbb{N}^{6602 \times 1}$ as the matrix of unique integer ids for each data point, $y \in \mathbb{R}^{6602 \times 1}$, where $y_{i,1} = y_1^{(i)}$ the matrix of coverage values for each data-point, $C \in \mathbb{R}^{6602 \times 3}$,

Variable	Description
y_p	Proportion (0-1) of cheat cheat grass cover.
y_c	Cover class. 0 if $y_r \leq 0.2$, 1 otherwise.

Table 4: Prediction Targets

Variable	Description
c_1	Soil temperature and moisture regime class value.
c_2	Categorical value for vegetation cover type generalized from LANDFIRE (www.landfire.gov) vegetation data. 15 classes.
c_3	EPA Level III Ecoregions.

Table 5: Categorical Variables

where $\mathbf{C}_{i,j} = c_j^{(i)}$ the matrix of categorical variables associated with each data point, and $\mathbf{X} \in \mathbb{R}^{6602 \times 664}$, where $\mathbf{x}_{i,j} = x_j^{(i)}$. These values $\begin{bmatrix} \mathbf{w} & \mathbf{y} & \mathbf{C} & \mathbf{X} \end{bmatrix}$ are stored in comma delimited plain text csv format and may be accessed at <http://tobedetermined.gov>.

4 Methods

In our search for prospective models for producing high quality predictive maps at finest resolution across the full range of our study area, we explored regression models which predict the actual coverage of cheatgrass, as well as classification models. For the categorical mapping of cheatgrass occurrence, we chose two cover classes based on an evident separation in cheatgrass cover in the field data: 2% (low cover or absent) or cover > 2% (high cover or present). The location of field points colored by these classifications is shown in Figure 7. Continuous variables used in model development were standardized by subtracting the mean and then dividing by the standard deviation.

4.1 Baseline Models

For this study we explored two baseline methods for classification, Random Forest, and Linear Discriminant Analysis. We also explored two regression models, linear regression and a Random Forest regressor. For all baseline models, only the continuous variables were used as input. We used the implementation of Random Forest, Linear Discriminant Analysis, and Linear Regression provided in the Sci-kit learn python library.

4.2 Deep Learning Models

For deep learning models we use both RNN and DNN. Will add more to this.

4.2.1 Deep Neural Network

The deep neural network for classification and regression is depicted in Figure 8. I will add a more detailed description soon.

4.2.2 Recurrent Neural Network

The recurrent neural network for classification and regression is depicted in Figure 9. I will add a more detailed description soon.

Variable	Description
x_1	Latitude.
x_2	Longitude.
x_3	Elevation above sea level.
x_4	Potential Relative Radiation (available solar radiation for photosynthesis).
x_5	Long-term median cumulative winter precipitation based on PRISM.
x_6	Long-term median cumulative growing degree days (GDD), Oct-Apr.
$x_{7:18}$	Normal 30 year monthly max temperatures. Original study used month 5.
x_{19}	30-year normal annual maximum temperature.
$x_{20:31}$	30-year normal monthly min temperatures. Original study used months 3,11.
x_{32}	30-year normal annual minimum temperature.
$x_{33:44}$	30-year normal monthly precipitation for all months. Original study used months 3,6,7.
x_{45}	30-year normal annual precipitation.
x_{46}	Average of 30-year normal monthly maximum temperature during select winter months (Nov-Feb)
x_{47}	Cumulative precipitation during select winter season months (Dec-Feb).
x_{48}	Cumulative precipitation during select spring season months (Apr-May).
x_{49}	Cumulative precipitation during select summer season months (Jun-Sep).
x_{50}	30-year normal monthly minimum temperature during select winter months (Nov-Dec).
x_{51}	MODIS long-term median annual peak NDVI.
x_{52}	Delta NDVI (Normalized Difference Vegetation Index) from long term median peak NDVI in year of peak cumulative winter precipitation.
x_{53}	Landsat7 long-term median annual peak NDVI.
x_{54}	Landsat7 long-term median spring peak NDVI.
x_{55}	Landsat7 long-term median summer peak NDVI.
$x_{56:325}$	LandSat annual, spring, summer composite pixels.
$x_{326:661}$	MODIS annual, spring, summer composite pixels.
x_{662}	MODIS annual peak NDVI.
x_{663}	MODIS spring peak NDVI
x_{664}	MODIS summer peak NDVI.

Table 6: Continuous Variables. Shaded variables were used in making the original Linear Discriminant Analysis model.

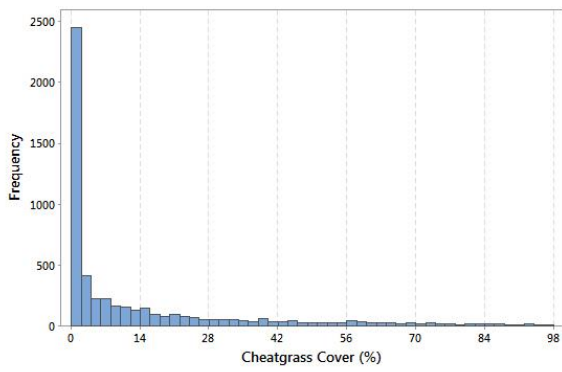


Figure 6: Histogram Showing Distribution of Cheatgrass Cover Values Measured at Field Locations.

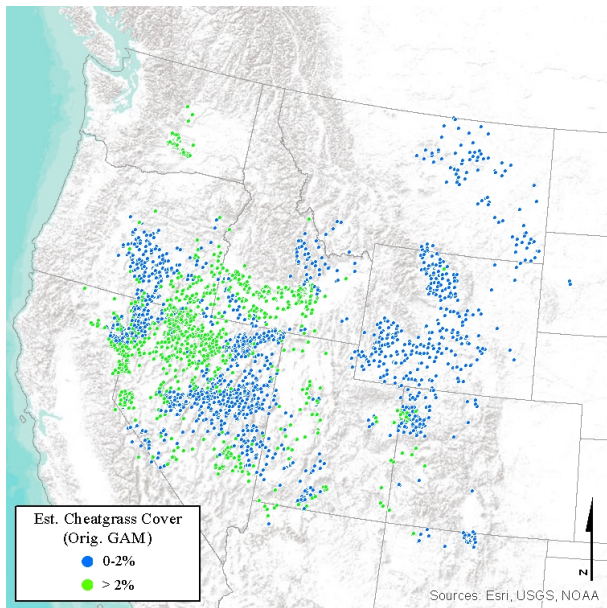


Figure 7: Classification of field samples

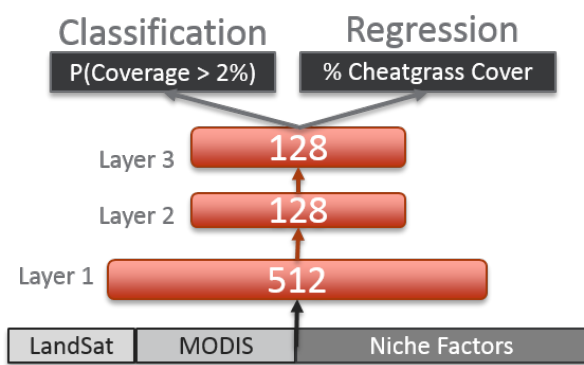


Figure 8: Deep Neural Network for Classification

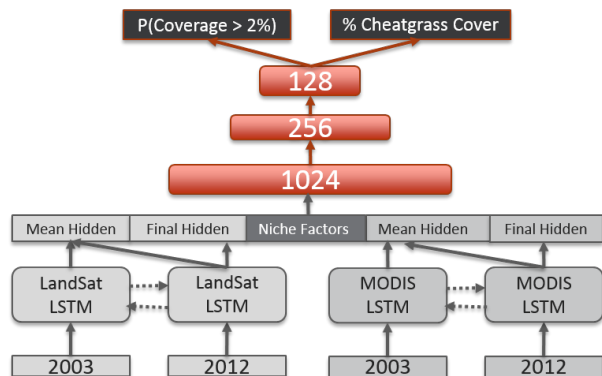


Figure 9: Recurrent Neural Network for Classification

	D_1	D_2	D_3	D_4
LR	0.1340	0.1115	0.1041	0.1059
RF	0.0913	0.0926	0.0909	0.0909
DNN	0.1006	0.0795	0.0787	0.0746
RNN	—	0.0790	0.0806	0.0766

Table 7: Mean Absolute Error for predicting cheat grass coverage.

	D_1	D_2	D_3	D_4
LDA	73.816	78.279	80.653	79.826
RF	80.897	81.142	82.736	82.643
DNN	79.604	82.004	82.456	83.203
RNN	—	81.388	81.820	82.597

Table 8: Classification accuracy of models for subsets of data

4.3 Performance on Field measurement locations

4.4 Experimental Setup

In order to gage the effectiveness of incorporating satellite data from multiple platforms we trained each prospective model on each of four subsets of the complete data. For the neural network models we also include the categorical variables for each subset of the data.

- D_1 : Ecological Niche Factors
- D_2 : Ecological Niche Factors + MODIS imagery
- D_3 : Ecological Niche Factors + LandSat imagery
- D_4 : All Variables.

We performed a random hyperparameter search for each prospective model. For each model we chose 200 random configurations of hyperparameters within reasonable ranges for performance and computation time. For each of these runs we tested performance using 5-fold stratified cross-validation where field data was split into each of the 5 folds with equal distributions over the different ecoregions and generalized land cover classifications.

5 Results and Analysis

In this section we discuss the results of experiments in turn. In section 5.1.1 we discuss performance of all models trained for the field locations in the dataset. Then we limit the scope of our analysis of the training performance for the best performing model. We continue to explore the strengths and weaknesses of the best performing model which we derive the final mapping product from in Section. Finally we explore the effectiveness of the final mapping product using ecological analysis.

5.1 Performance on Field measurement locations

In this section we report statistics on field measurement locations.

5.1.1 Quantitative assessment

Quantitative results are reported for the average performance across cross-validation folds for each of the 4 subsets of input variables. Tables 7 and 8 show the outcomes of experiments in terms of accuracy for regression and classification prediction respectively. We chose the best performing model in terms of accuracy to create the final mapping product, and for this model we report several classification statistics for each of the four input variable subsets in Table 9.

5.1.2 Training Statistics

In this section we analyse training statistics for the best performing model. Discussion to be provided soon.

	Precision	Recall	F-score	AUC	Accuracy	Std. Accuracy
D_1	0.795	0.820	0.808	0.866	0.796	0.025
D_2	0.844	0.803	0.823	0.893	0.820	0.014
D_3	0.831	0.833	0.832	0.900	0.825	0.015
D_4	0.837	0.842	0.839	0.902	0.832	0.012

Table 9: Performance across a range of metrics for most accurate DNN models for each subset of input variables.

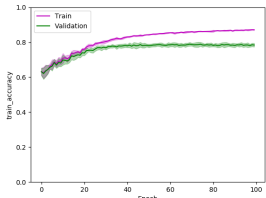


Figure 10: D_1

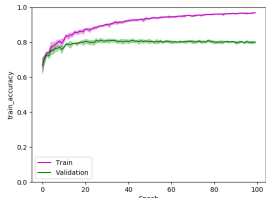


Figure 11: D_2

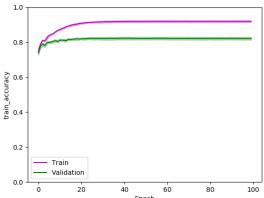


Figure 12: D_3

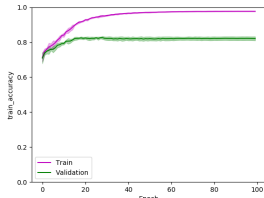


Figure 13: D_4

Figure 14: Train versus test accuracy over epochs for input variable subsets

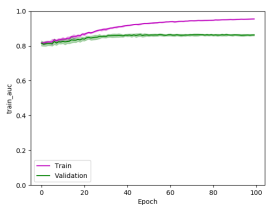


Figure 15: D_1

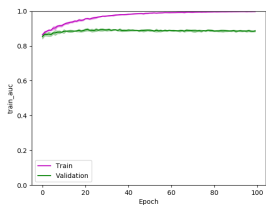


Figure 16: D_2

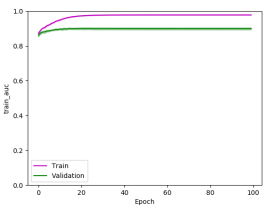


Figure 17: D_3

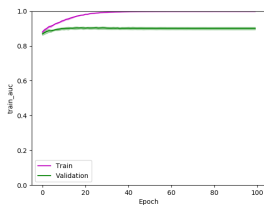


Figure 18: D_4

Figure 19: Train versus test area under the ROC curve over epochs for input variable subsets

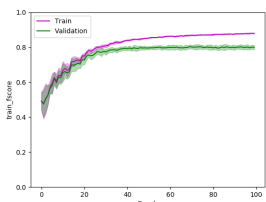


Figure 20: D_1

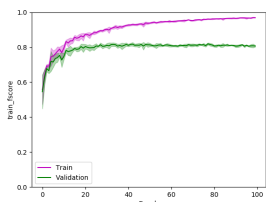


Figure 21: D_2

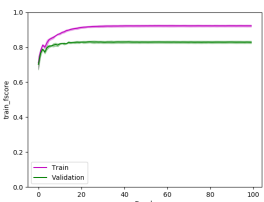


Figure 22: D_3

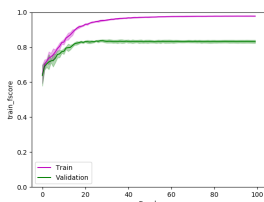


Figure 23: D_4

Figure 24: Train versus test F-score over epochs for input variable subsets

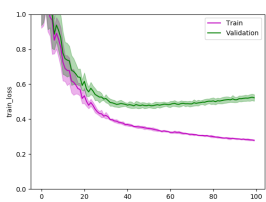


Figure 25: D_1

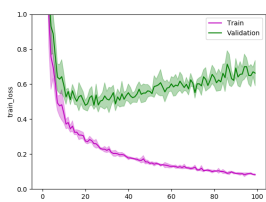


Figure 26: D_2

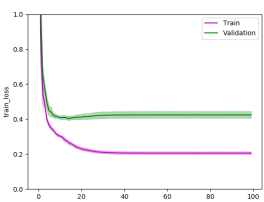


Figure 27: D_3

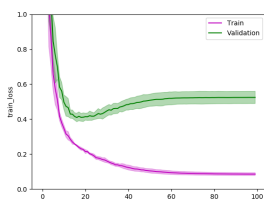


Figure 28: D_4

Figure 29: Train versus test cross entropy loss over epochs for input variable subsets

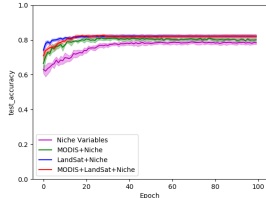


Figure 30: Accuracy

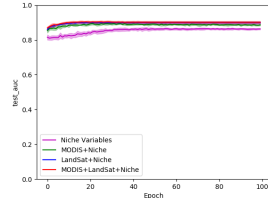


Figure 31: Area under ROC

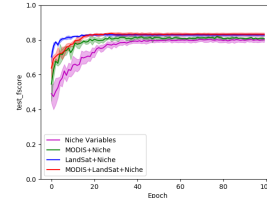


Figure 32: F-score

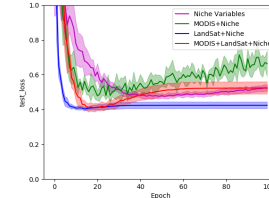


Figure 33: Cross-entropy

Figure 34: Test metrics plotted for input variable subsets

5.1.3 Qualitative assessment

- Confusion Matrix
- Histograms according to true coverage and variables of interest
- Map of field data symbolized by classification error

5.2 Performance on Full Study Region

In this section we analyze the geographic variability in cross-validation model predictions among other things.

5.2.1 Pixel-wise count of cheatgrass class across model predictions

5.2.2 Block statistics (count) of cheatgrass class (analogous to block area), then look at range of block counts

6 Conclusion and Future Work

References

- [1] ADAM, E., MUTANGA, O., AND RUGEGE, D. Multispectral and hyperspectral remote sensing for identification and mapping of wetland vegetation: a review. *Wetlands Ecology and Management* 18, 3 (2010), 281–296.
- [2] BELLUCO, E., CAMUFFO, M., FERRARI, S., MODENESE, L., SILVESTRI, S., MARANI, A., AND MARANI, M. Mapping salt-marsh vegetation by multispectral and hyperspectral remote sensing. *Remote sensing of environment* 105, 1 (2006), 54–67.
- [3] CE, C. Ecological regions of north america: toward a common perspective.
- [4] GOVENDER, M., CHETTY, K., AND BULCOCK, H. A review of hyperspectral remote sensing and its application in vegetation and water resource studies. *Water Sa* 33, 2 (2007), 145–151.
- [5] HESTIR, E. L., KHANNA, S., ANDREW, M. E., SANTOS, M. J., VIERS, J. H., GREENBERG, J. A., RAJAPAKSE, S. S., AND USTIN, S. L. Identification of invasive vegetation using hyperspectral remote sensing in the california delta ecosystem. *Remote Sensing of Environment* 112, 11 (2008), 4034–4047.
- [6] JEEVALAKSHMI, D., REDDY, S. N., AND MANIKIAM, B. Land cover classification based on ndvi using landsat8 time series: A case study tirupati region. In *Communication and Signal Processing (ICCSP), 2016 International Conference on* (2016), IEEE, pp. 1332–1335.
- [7] OMERNIK, J. M., AND GRIFFITH, G. E. Ecoregions of the conterminous united states: evolution of a hierarchical spatial framework. *Environmental management* 54, 6 (2014), 1249–1266.
- [8] SALEQUZZAMAN, M. Ecoregions: A spatial framework for environmental management. *Water Encyclopedia* 2 (2005), 667–668.
- [9] THENKABAIL, P. S., AND LYON, J. G. *Hyperspectral remote sensing of vegetation*. CRC Press, 2016.
- [10] USGS, D. Landsat surface reflectance-derived spectral indices, 2014.

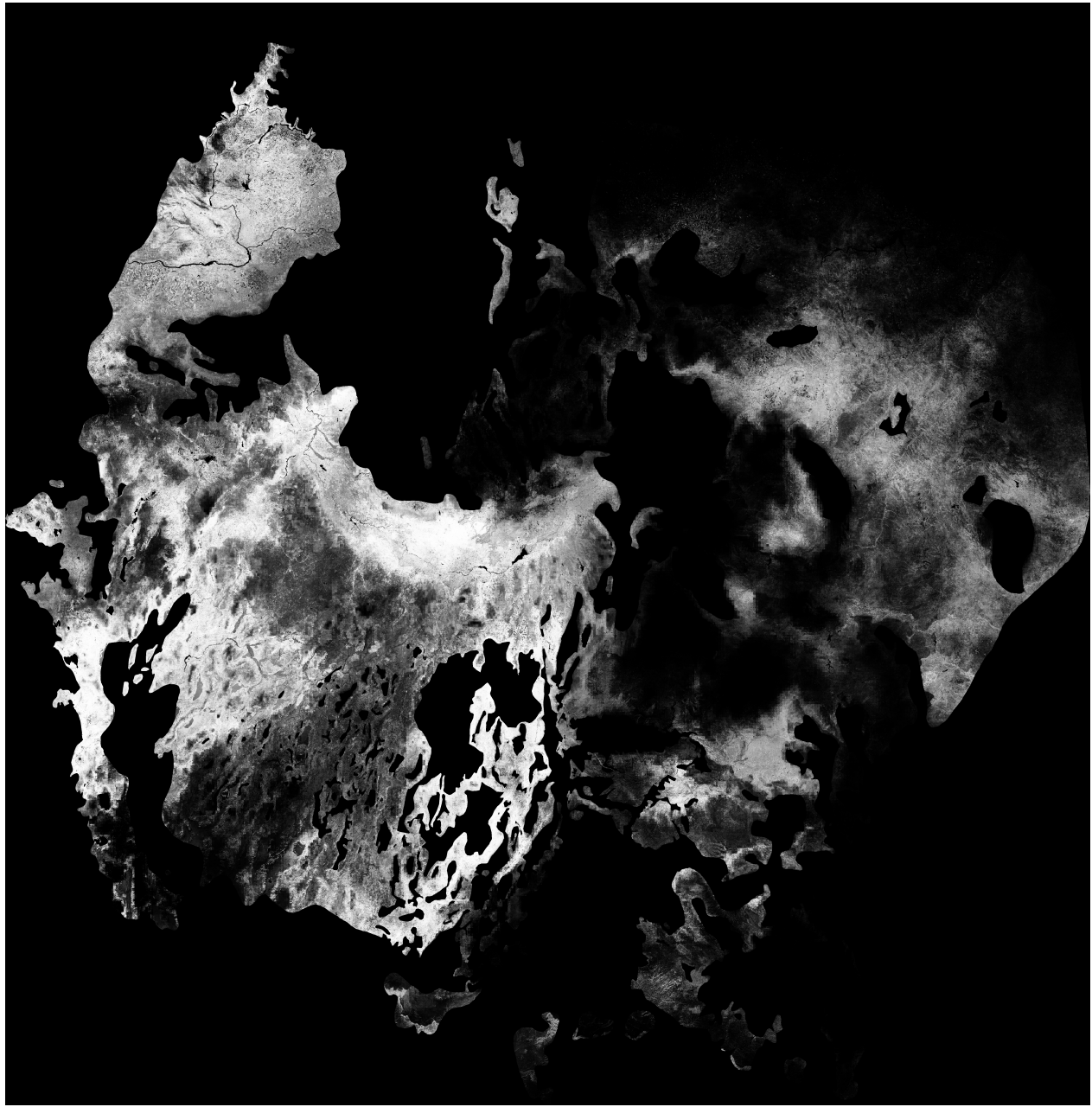


Figure 35: 250 meter resolution map for best deep neural network classification model.